EFFECT OF HUMIDIY ON LONG FATIGUE LIFE MORE THAN 10^7 CYCLES IN HIGH STRENGTH STEEL

M. Nakajima [1], K. Tokaji [2] and T. Shimizu [1]

[1] Department of Mechanical Engineering, Toyota National College of Technology,
2-1 Eisei-cho, Toyota 471-8525, Japan
[2] Department of Mechanical and Systems Engineering, Faculty of Engineering, Gifu University,
1-1 Yanagido, Gifu 501-1193, Japan

ABSTRACT

Long-term fatigue tests have been conducted in order to clarify the effect of humidity on the fracture mechanism in long life region more than 10^7 cycles. The material used was a low alloy steel, JIS SNCM439 (AISI4340). Tests were performed using cantilever-type rotating bending fatigue testing machines operating at a frequency of 3150rpm in laboratory air and in dry air. The dew point of dry air was – 60°C In laboratory air, fatigue failure occurred at stress levels below the conventional fatigue limit, leading to a step-wise *S-N* curve. Also in dry air, the similar step-wise *S-N* curve was obtained, but the position of the horizontal line in the *S-N* curve shifted to high stress level *i.e.* short life region. Fracture mode at stress levels below the horizontal line was fish-eye type in both environments, *i.e*. cracks were initiated from a nonmetallic inclusion at subsurface. Since two different fracture modes, *i.e*. surface slip type and fish-eye type, coexisted, fatigue life distribution was scattered at the stress level of the horizontal line. Therefore, it is concluded that the appearance of horizontal line was due to the scatter of fatigue life corresponding to the fracture mode.

INTRODUCTION

It has been indicated that fatigue failure often occurred at stress levels below the conventional fatigue limit in long life region [1-3], particularly seen in high strength steels and surface-treated steels [4]. Provided design is conducted in accordance with the fatigue limit, the reliability of machine components could be faced with a difficulty by the above aspect. Such a failure is known to be caused by fish-eye which is developed from a nonmetallic inclusion in the interior of materials [1-4]. Furthermore, high strength steel is sensitive to the aqueous environments and hydrogen embrittlement is caused by the humidity in air [5]. It is recently indicated that the formation of fish-eye can be related to the environmental effects such as hydrogen embrittlement [6]. However, the source of this hydrogen is unidentified whether it is picked up in the manufacturing process or during fatigue test. If hydrogen is picked up during fatigue test, it is expected that the experiments in dry air would bring the interesting results which are different from those obtained in laboratory air. Many studies have been performed on the characteristic fatigue behaviour, while the effect of humidity on the fracture mechanism in long life region has not been fully understood. In addition, although fatigue testing machines operating at a high frequency more than 10^4 Hz are used to save the time in high cycle fatigue [1-2,7], most of the machine components are not subjected to such a high frequency of stress fluctuation. Moreover, it becomes difficult to detect the environmental effects in short time fatigue tests. Accordingly, it seems that fatigue testing machine operating at a moderate frequency should be used, while much time would be spent.

In the present study, fatigue tests were carried out in order to clarify the effect of humidity on the fracture mechanism in long life region more than 10^7 cycles. Special emphasis is placed on subsurface crack initiation mechanism.

EXPERIMENTAL PROCEDURES

The material used is a low alloy steel, JIS SNCM439 (AISI 4340), which was oil-quenched at 880°C and then tempered at 200°C and 500°C; hereafter they are designated as QT200 and QT500, respectively. The mechanical properties are given in Table 1. After heat treatment, round bar specimens with a diameter of 3.5 mm as shown in Fig.1 were machined. Specimens were polished by emery paper and then buff-finished using chromic oxide (Cr_2O_3) before fatigue testing. Fatigue tests were performed using cantilever-type rotating bending fatigue testing machines operating at a frequency of 3150rpm in laboratory air and in dry air. The dew point of dry air was – 60°C. Fracture surfaces of all specimens were examined using a scanning electron microscope (SEM).

TABLE 1
MECHANICAL PROPERTIES

Tempering temperature	0.2% proof stress $\sigma_{0.2}$ MPa	Tensile strength σ_B MPa	Breaking strength on final area σ_T MPa	Elongation δ %	Reduction of area φ %	Vickers hardness HV
200°C	**1490**	**1863**	**2561**	**9**	**45**	**462**
500°C	**1158**	**1226**	**1909**	**10**	**56**	**379**

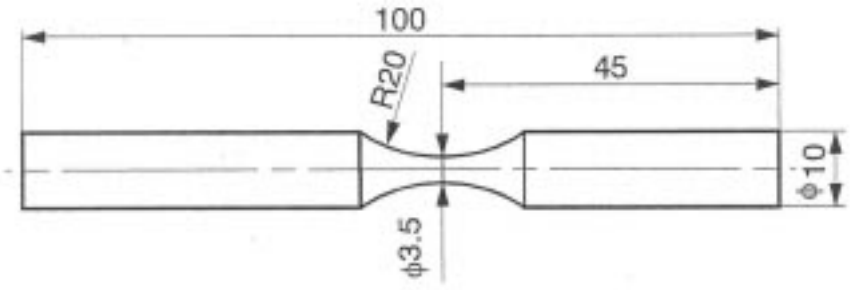

Figure 1: Specimen configurations

RESULTS

S-N Curves

Figure 2 shows the *S-N* curve obtained in laboratory air for QT200. Although the conventional fatigue limit (σ=1000MPa : horizontal line) is seen, fatigue failure occurred at stress levels below the fatigue limit in long life region. A step-wise *S-N* curve was obtained, and the fracture mode at stress levels below the fatigue limit was fish-eye type, *i.e.* cracks were initiated from a nonmetallic inclusion at subsurface, while surface slip type was found above the fatigue limit. Two different fracture modes, *i.e.* surface slip type and fish-eye type, coexisted at the fatigue limit, and fish-eye type failure can be seen in longer life region.

The *S-N* curve obtained in dry air for QT200 is shown in Fig.3. Also in dry air, the similar step-wise *S-N* curve is seen, but the position of the horizontal line in the *S-N* curve shifted to high stress level (σ=1200MPa), *i.e.* short life region. This horizontal line in dry air is not regarded as the fatigue limit and the fracture mode was fish-eye type below the horizontal line, while was surface slip type above it. In addition, two different fracture modes coexist at the horizontal line.

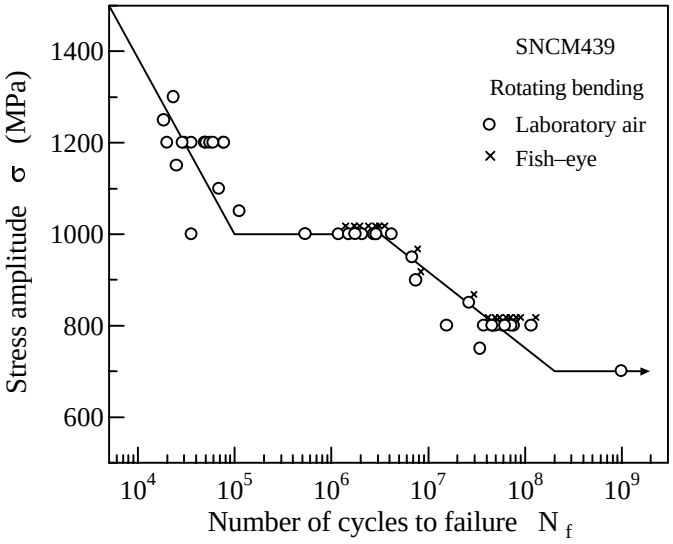

Figure 2: *S-N* curve in laboratory

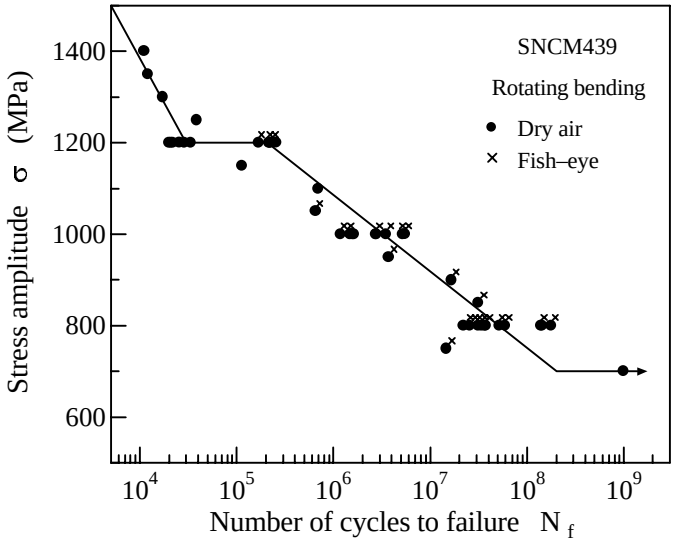

Figure 3: *S-N* curve in dry air

For comparison, the *S-N* curves in laboratory air and in dry air were plotted in Fig.4. Fatigue lives above the horizontal line in dry air are almost the same in both environments. In this region, the fatigue life is so short, thus laboratory air exerted no influence on fatigue life. In the long life region below the horizontal line in laboratory air, the fracture mode changes from surface to interior, thus it is expected that the effect of humidity on the fatigue life does not appear. Therefore, the difference in fatigue lives between laboratory air and dry air appears in the region between two horizontal lines. The specimens which did not fail at 10^9 cycles at 700MPa in both environments were broken in liquid nitrogen and the fracture surfaces were closely examined by SEM. The results will be described later.

The results of QT500 obtained in laboratory air and in dry air show the conventional *S-N* curves, *i.e.* a step-wise *S-N* curve was not observed and the conventional fatigue limit was established in the range up to 2×10^8 cycles. Thus fatigue failure did not occur at stress levels below the fatigue limit. Fatigue lives and fatigue limit in dry air are superior compared with those in laboratory air. The fatigue limits in laboratory air and in dry air are 625MPa and 650MPa, respectively. From SEM observation, the fracture mode of QT500 was surface slip type in all specimens, *i.e.* no fish-eye type fracture was observed. Based on the results, it is suggested that the conventional fatigue limit appears in high strength steels with Vickers hardness less than *HV*400.

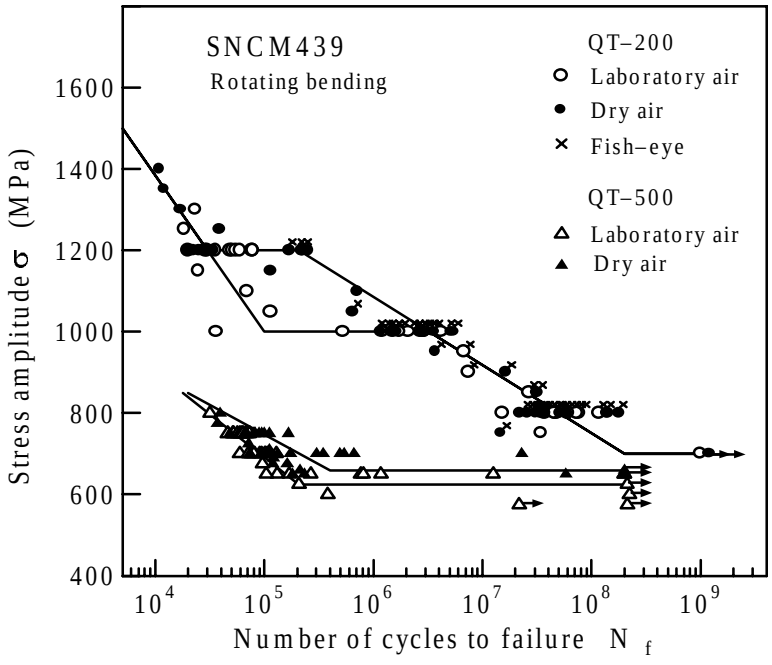

Figure 4: *S-N* curves in laboratory air and in dry air

Fatigue Life Distribution

Fatigue life distributions were examined at three stress levels in laboratory air and in dry air, and 10 specimens were allocated to each stress level. The results were plotted on a Weibull probability paper as shown in Fig.5 and analyzed by a three-parameter Weibull distribution. The obtained distribution functions are represented by the solid line in the figure, showing a good correlation with the experimental data. It is known that the characteristics of fatigue life distributions are strongly dependent on fracture mode. The discontinuity of the distribution is seen at σ=1000MPa in laboratory air and at σ=1200MPa in dry air. Microscopic observation on fracture surfaces revealed that two different fracture modes, *i.e*. surface slip type and fish-eye type, coexisted at those stress levels. Therefore, the distributions were re-analyzed using a mixed Weibull distribution.

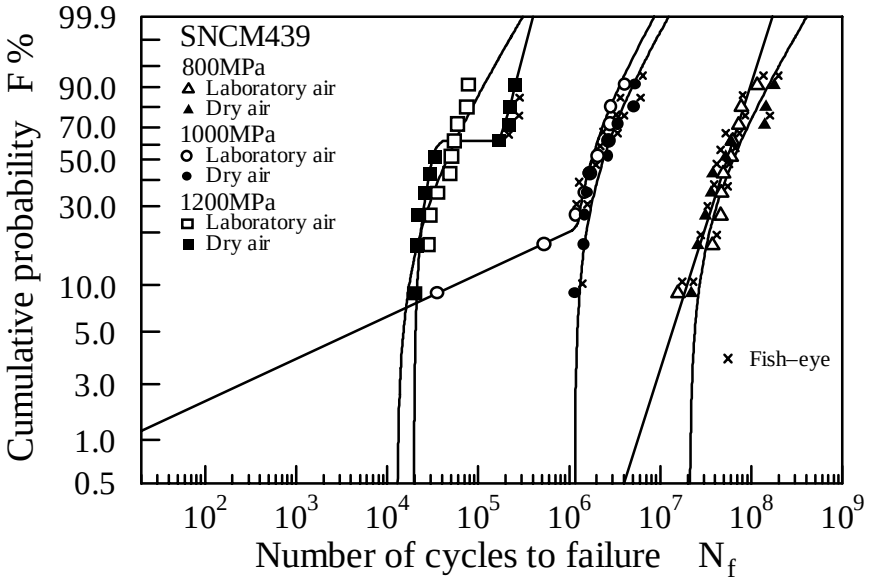

Figure 5: Fatigue life distributions plotted on Weibull probability paper

At σ=800MPa, the fatigue life distributions in both environments are almost the same. Although the conventional fatigue limit was seen in laboratory air at σ=1000MPa, the fatigue lives are scattered as described previously. The fatigue life distributions in both environments are almost similar except for two data points in laboratory air. The same tendency is also found at σ=1200MPa, *i.e*. except for four data points in dry air, the both distributions are similar. Therefore, it is confirmed that the appearance of the horizontal line in the *S-N* curves is due to the scatter of fatigue life corresponding to the coexistence of two fracture modes.

Quantitative Analysis of Fish-eye

Fish-eye fracture was examined in detail using SEM. From the observation of all the specimens, fish-eye was inscribed with the specimen surface, and nonmetallic inclusion was recognized at the center of fish-eye. Figure 6 shows the relationship between the depth from surface to inclusion, d_{inc}, and the number of cycles to failure, N_f. The data obtained are considerably scattered and the correlation between both is not observed. However, most of inclusions are located within 0.12mm from the specimen surface irrespective of the environment. It seems to be dependent on the loading condition of bending, *i.e*. stress gradient.

Fish-eyes were analyzed quantitatively using $\sqrt{(area)}$ method proposed by Murakami *et al*.[8]. The sizes of inclusion and fish-eye were measured, and the geometrical parameter, $\sqrt{(area)}$, was calculated as a representative size. Figure 7 shows the relationships between $\sqrt{(area)}$ and N_f. The sizes of inclusion calculated by the $\sqrt{(area)}$ method are almost constant regardless of N_f. On the other hand, the sizes of fish-eye are scattered and the correlation between both is not observed. It is also seen that the sizes of inclusion and fish-eye are not dependent on the environment.

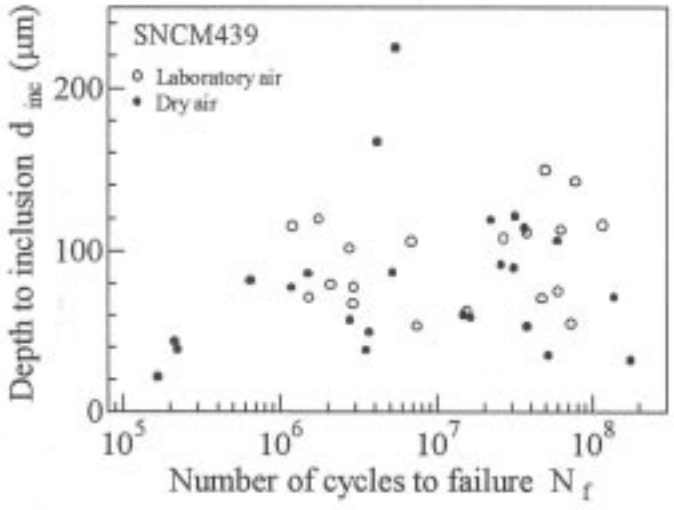

Figure 6: Relationship between d_{inc} and N_f

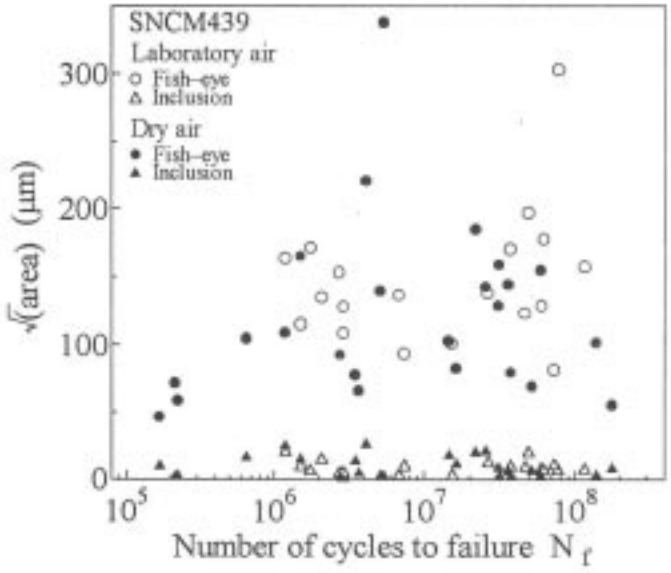

Figure 7: Relationship between $\sqrt{area}$ and N_f

Based on the results in Fig.7, the initial stress intensity factor range, ΔK_{ini}, for crack initiation from the inclusion and for the transition from fish-eye to surface crack was evaluated by the following equations, respectively;

$$\Delta K_{ini}=0.5\sigma_{at}\sqrt{\pi\sqrt{area}} \quad (1)$$

$$\Delta K_{ini}=0.65\sigma_{a}\sqrt{\pi\sqrt{area}} \quad (2)$$

where $\Delta K=K_{max}$ because stress ratio is – 1, σ_{at} is the stress at the inclusion site and σ_a is the nominal stress. Figure 8 shows the relationships between ΔK_{ini} and N_f. The ΔK_{ini} for crack initiation from the inclusion is almost the constant with increasing fatigue life, *i.e.* 1.0~4.2MPa$\sqrt{m}^{1/2}$. On the other hand, the ΔK_{ini} for the transition from fish-eye to surface crack shows a considerable scatter.

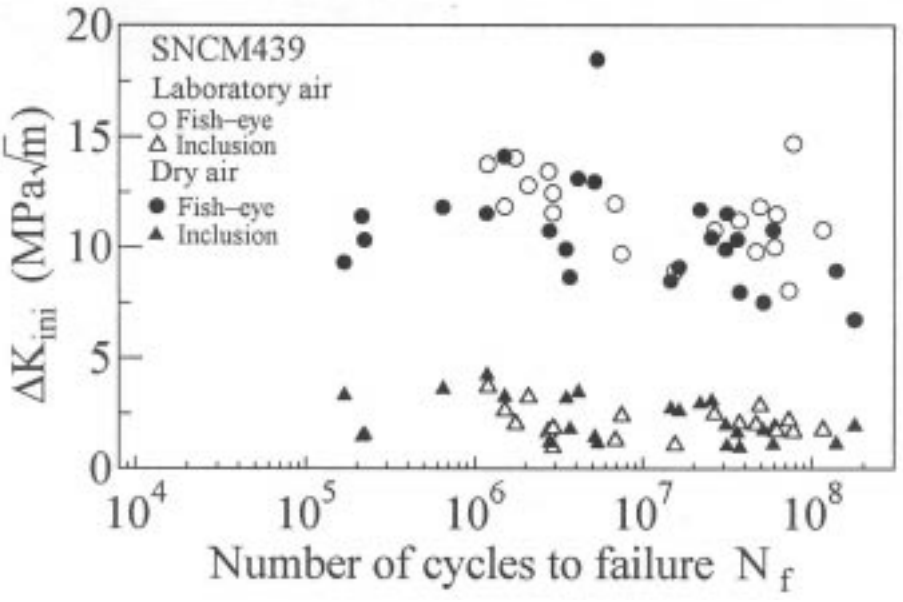

Figure 8: Relationships between ΔK_{ini} and N_f

DISCUSSION

Mechanism of Subsurface Crack Initiation

Based on the results, a model of the fatigue failure at stress levels under the conventional fatigue limit is now

proposed. Figure 9 represents the schematic illustration of stress distribution surrounding the inclusion in bending.

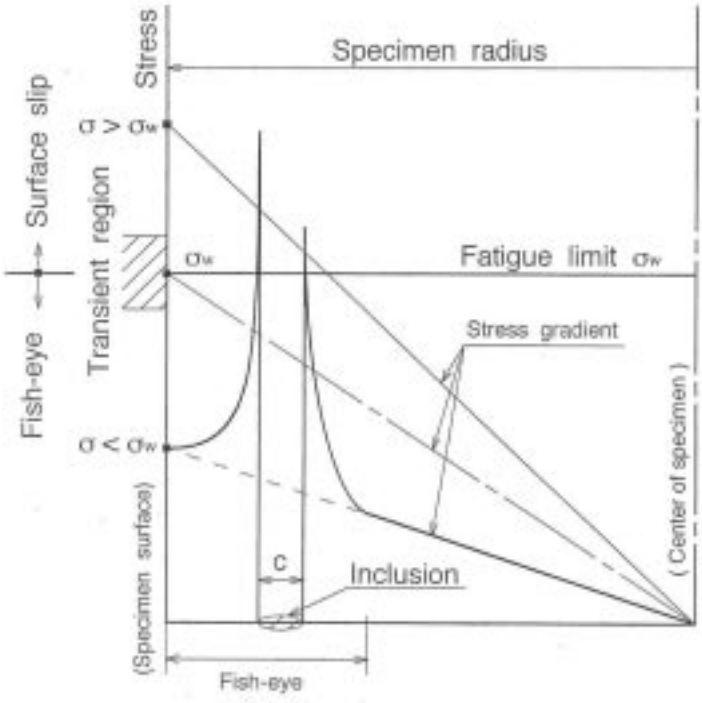

Figure 9: Schematic illustration of stress distribution surrounding inclusion in bending

First of all, it is assumed that the deformation is not easier in subsurface region than surface, because the deformation is constraint in subsurface region. In other words, the priority of fracture is given to surface. When stress levels above the fatigue limit (σ_w) are applied, failure occurs by surface slip. Although the high stress should be generated around the inclusion by means of stress concentration, since the deformation is easier at surface than subsurface region, failure occurs at surface. However, in surface hardened materials, *i.e.* carburized and nitrided materials, fish-eye fracture also takes place at stress levels above the fatigue limit. When stress levels are around the fatigue limit, failure occurs by means of either surface slip or fish-eye as shown in Fig.2 and 3. Two fracture modes coexist at the fatigue limit, and fish-eye type failure is found in a long life region. When stress levels are below the fatigue limit, failure occurs by means of fish-eye in subsurface region, because failure at surface no longer takes place, *i.e.* stress levels are too low to generate the surface slip. At this time, the higher stress more than the fatigue limit should be generated in the vicinity of the inclusion by stress concentration. This is the mechanism of fish-eye type fracture in long life region. In this mechanism, it is important whether the plastic deformation is generated or not around the inclusion by means of stress concentration. Therefore, this type of fracture is not seen in the low strength materials. It seems that the humidity in air enhances the crack initiation on the surface.

Failure Mechanisms and a Form of S-N Curve

Figure 10 represents the schematic illustration of the form of the *S-N* curve for high strength steels with a change in environment. In laboratory air, a step-wise *S-N* curve is seen and fracture modes above and below the fatigue limit are surface slip and fish-eye, respectively. Two different fracture modes coexist at the fatigue limit, thus the scatter of the fatigue lives becomes large. From these results, the appearance of the fatigue limits in high strength steels is due to the scatter of fatigue life corresponding to the coexistence of two fracture modes. Therefore, specimens would have to failure, provided the experiments is kept going on beyond 10^7 cycles. Also in dry air, the similar step-wise *S-N* curve is obtained, but the position of the horizontal line in the *S-N* curve shifts to high stress level, *i.e.* short life region. This horizontal line is not regarded as the fatigue limit, because of short fatigue lives less than 10^7 cycles. However, at this stress level, two fracture modes coexist as well as in laboratory air. Above this stress level, fatigue lives in both environments are almost the same and the fracture mode is surface slip type.

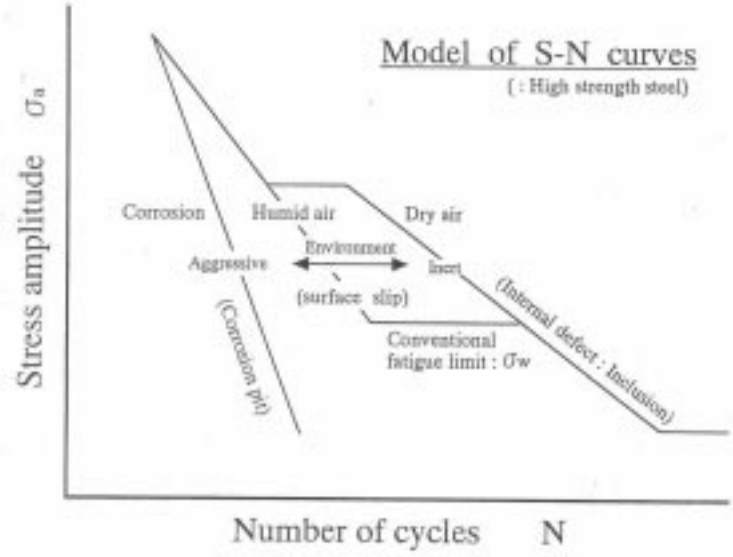

Figure 10: Schematic illustration of *S-N* curves

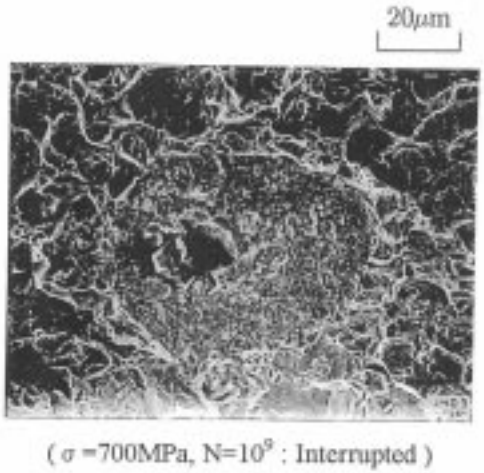

Figure 11: SEM micrograph of fish-eye observed at 10^9 cycles

Also in long fatigue life region more than 10^7 cycles, fatigue lives in both environments become similar, because of the transition of fracture mode from surface to interior. When stress level is further decreased, the secondary fatigue limit would be expected to appear at gigacycle region. Figure 11 shows SEM micrograph of the fish-eye observed in the specimen which was interrupted at 10^9 cycles in laboratory air. The $\sqrt{(area)}$ of fish-eye is 48μm, and the depth to inclusion is 157μm. Since the specimen was broken in liquid nitrogen, the fish-eye is surrounding by brittle feature. It is unclear whether this fish-eye is non-propagating one or not. Therefore, unless confirmed non-propagating, the secondary fatigue limit could exist at lower stress level.

Schematically illustrated *S-N* curve in a corrosive environment is also given in Fig.10. In steels except for stainless steels, since the corrosion pits are generated on surface in aqueous environments, the fatigue lives would decrease, and it seems that the fracture mode does not change from surface to interior. However, these are the subjects in the future.

CONCLUSIONS

Long-term fatigue tests have been conducted in order to clarify the effect of humidity on the fracture mechanism in laboratory air and dry air using a high strength steel, JIS SNCM439 (AISI4340). The results obtained are as follows;

(1) In laboratory air, fatigue failure occurred at a stress level below the conventional fatigue limit, leading to a step-wise *S-N* curve. Also in dry air, the similar step-wise *S-N* curve was obtained, but the position of the horizontal line in the *S-N* curve shifted to high stress level. *i.e.* short life region.
(2) In both environments, fracture mode was fish-eye type at stress levels below the horizontal line, while it was surface slip type above the horizontal line. In addition, two fracture modes, *i.e.* surface slip and fish-eye, coexisted at the horizontal line.
(3) Since two fracture modes coexisted, fatigue life distribution was considerably scattered at the stress level of the horizontal line. Therefore, it is concluded that the appearance of the horizontal line was due to the scatter of fatigue life corresponding to the fracture mode.
(4) The initial stress intensity factor ranges for crack initiation from the inclusion are almost the constant regardless of fatigue life, *i.e.* 1.0~4.2MPa$\sqrt{\mathrm{m}}$. On the other hand, the stress intensity factor ranges for the transition from fish-eye to surface crack indicated a considerable scatter and no correlation between both was seen.

REFERENCES

1. Bathias, C. (1999) *Fatigue Fract. Engng Mater. Struct.* **22**, 559.
2. Wang, Q. Y., Berard, J. Y., Dubarre, A., Baudry, G., Rathery, S. and Bathias, C. (1999) *Fatigue Fract. Engng Mater. Struct*. **22**, 667.
3. Emura, H. and Asami, K. (1989) *Trans. Jpn Soc.Mech.Eng*. **A-55**, 45. (in Japanese)
4. Shiozawa, K., Nishino, S., Ohtani, T. and Mizuno, S. (1998). In: *Small Fatigue Cracks*: *Mechanics and Mechanisms*, pp.6-11.
5. Endo, K., Komai, K. and Imashiro, N. (1976) *Trans. Jpn Soc.Mech.Eng*. **42**, 2652. (in Japanese)
6. Murakami, Y., Nomoto, T. and Ueda, T. (1999) *Fatigue Fract. Engng Mater. Struct*. **22**, 581.
7. Bathias, C. and Ni, J. (1993) *ASTM STP 1211*, pp.141-152.
8. Murakami, Y., Kodama, S. and Konuma, S. (1988) *Trans. Jpn Soc.Mech.Eng*. **A-54**, 688. (in Japanese)